# RESTORING FORCE CHARACTERISTICS EVALUATION FOR STEEL CONCRETE COMPOSITE COLUMNS WITHOUT COVER CONCRETE

K. Sadasue[1]

[1] *Associate Professor, Hiroshima Institute of Technology, sadasue@cc.it-hiroshima.ac.jp*

## *Abstract*

A steel reinforced concrete structure possesses the properties of both concrete and steel, and by having an appropriate design it is possible for such a structure to provide good earthquake resistance. High-rise concrete buildings with steel reinforcements displayed a good earthquake-resistance capacity when subjected to the Kanto earthquake (1923) as compared to ordinary reinforcements. Since then, the encased structural system, which is a form of composite construction, has been employed in Japan for most building frames taller than seven stories. However, the construction of ordinarily steel reinforced concrete buildings has decreased because of the demand for the reduction of the construction cost. That is because steel reinforced concrete structures used the steel, it is higher than reinforced concrete structures on both sides of material cost and construction cost. This situation is that the excellent mechanical property of steel concrete composite structure cannot be used. Thus, this research investigates how steel concrete composite columns can be earthquake-resistant, workable, and economical. Proposed new type steel concrete composite structure which can be used by changing into reinforced concrete structure is the best use of the characteristic of steel reinforced concrete columns and concrete filled steel tubular columns.

This paper discusses steel concrete composite columns without cover concrete. The mechanical behavior of the columns with symmetric and asymmetric cross sections was confirmed through seismic loading tests under a constant vertical load. The test specimens were cantilever that assumes the behavior below the inflection point of the column. The experimental parameters were axial force ratio and shape of the steel. All the test specimens were designed so that failure under flexure occurred earlier than failure under shear. The test results showed that under the hysteresis characteristics of the columns with a symmetrical cross section under low axial compression, the hysteresis loop indicated a spindle-shape. Moreover, large ductility and a small amount of degradation in the strength due to repeated loading was observed. At the hysteresis characteristics of columns with an asymmetrical cross section, it is observed that the hysteresis loop indicated a spindle-shape with some pinching, and columns under low axial compression displayed ductility. On the other hand, under the hysteresis characteristics of the columns with a symmetrical cross section under high axial compression, drastic strength deterioration after reaching the maximum carrying capacity was seen. Furthermore, a reduction in the deformation capacity became remarkable for the columns with an asymmetrical cross section. The structural tests made it clear that ultimate flexural strength could be evaluated by the superposed strength method, in which the ultimate strength of the steel flange, steel web and concrete. Moreover, we showed that the proposed evaluation method of restoring force characteristics matches the test result well.

*Keywords: steel concrete; asymmetric cross section; ultimate flexural strength; hysteresis curve*

# 1. Introduction

A steel concrete composite structure possesses the properties of both steel and concrete, and by having an appropriate design it is possible for such a structure to provide good earthquake resistance. High-rise concrete buildings with steel reinforcements exhibited a good earthquake-resistant capacity during the Kanto earthquake (1923) as compared to concrete structures with ordinary reinforcements. Since then, the encased structural system, which is a form of steel concrete composite construction, has been employed in Japan for most building frames taller than seven stories. However, the construction of ordinarily steel reinforced concrete buildings has decreased because of the demand for the reduction of the construction cost. That is because steel reinforced concrete structures used the steel, it is higher than reinforced concrete structures on both sides of material cost and construction cost. This situation is that the excellent mechanical property of steel concrete composite structure cannot be used. Thus, this research investigates how steel concrete composite columns can be earthquake-resistant, workable, and economical. Fig.1 shows a new type of steel concrete composite columns. This new type steel concrete composite structure which can be used by changing into reinforced concrete structure is the best use of the characteristic of steel reinforced concrete columns and concrete filled steel tubular columns [1, 2]. It is also necessary to examine a column with an asymmetrical cross section to establish the design method of the new steel concrete composite structures.

Fig.1 (b-c) shows steel concrete composite columns with an asymmetrical cross section. For columns at the corner and the side positions of steel reinforced concrete buildings, the steel embedded in concrete is often composed of an asymmetrical section. These design methods are demanded similarly for new types of steel concrete composite structures. This paper presents the results of experiments carried out to study the mechanical behavior of steel concrete composite columns with symmetrical and asymmetrical cross sections under a constant axial load and a cyclic lateral load. This study mainly focuses on the destruction state, ultimate flexural strength, and hysteresis characteristics.

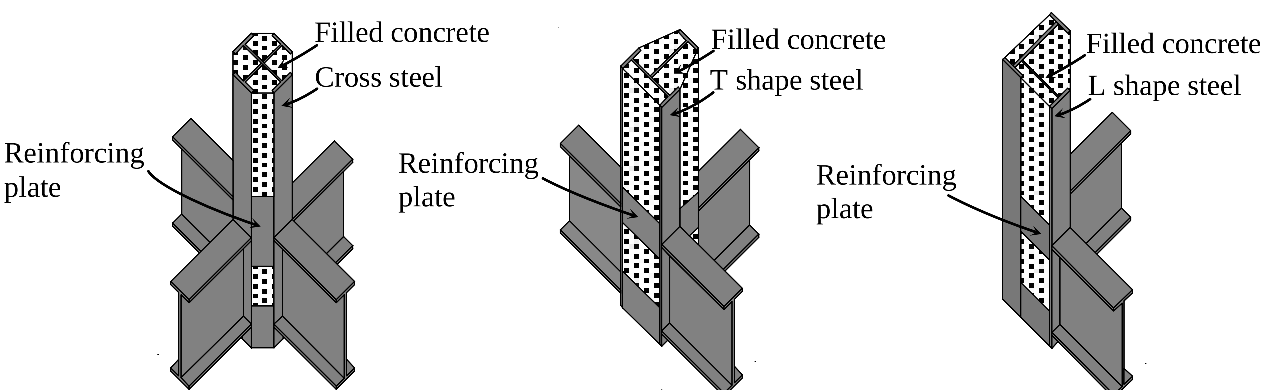


Fig. 1 – Steel concrete composite columns

# 2. Experimental work

## 2.1 Test specimens and loading system

The test specimens are cantilever that assumes the behavior below the inflection point of the column. A total of 10 specimens were tested to investigate the elasto-plastic flexural behavior of steel concrete composite columns with symmetrical and asymmetrical cross section. All test specimens were designed so that failure under flexure occurred earlier than failure under shear.

Table 1 shows the test program. The steel shape and dimensions are shown in Fig. 2. The test specimens had the column dimensions of 300mm×300mm; the column steel used H-300×150×6.5×9 (test series I: Grade SN400B, test series II, III: Grade SS400); and the reinforcing plates at the column base used PL-6(SS400). The following experimental parameters were selected:

Table 1 – Test program

| Specimen | Steel | $n$ | $N$ (kN) | $N_{cu}$ (kN) | ${}_cN_{cu}$ (kN) | ${}_sN_{cu}$ (kN) | Test Series |
|---|---|---|---|---|---|---|---|
| C01 | Cross shape | 0.12 | 724 | 6094 | 3376 | 2718 | I |
| TX01 | T shape | | 655 | 5504 | 3154 | 2350 | II |
| TY01 | | | | | | | |
| LX01 | L shape | | | | | | |
| LY01 | | | | | | | |
| C05 | Cross shape | 0.50 | 2809 | 5617 | 2599 | 3018 | III |
| TX05 | T shape | | 2517 | 5035 | | 2436 | |
| TY05 | | | | | | | |
| LX05 | L shape | | | | | | |
| LY05 | | | | | | | |

$n$: Axial force ratio
$N$: Axial force
$N_{cu}$: Compressive strength of steel concrete composite column
${}_cN_{cu}$: Compressive strength of concrete
${}_sN_{cu}$: Compressive strength of steel

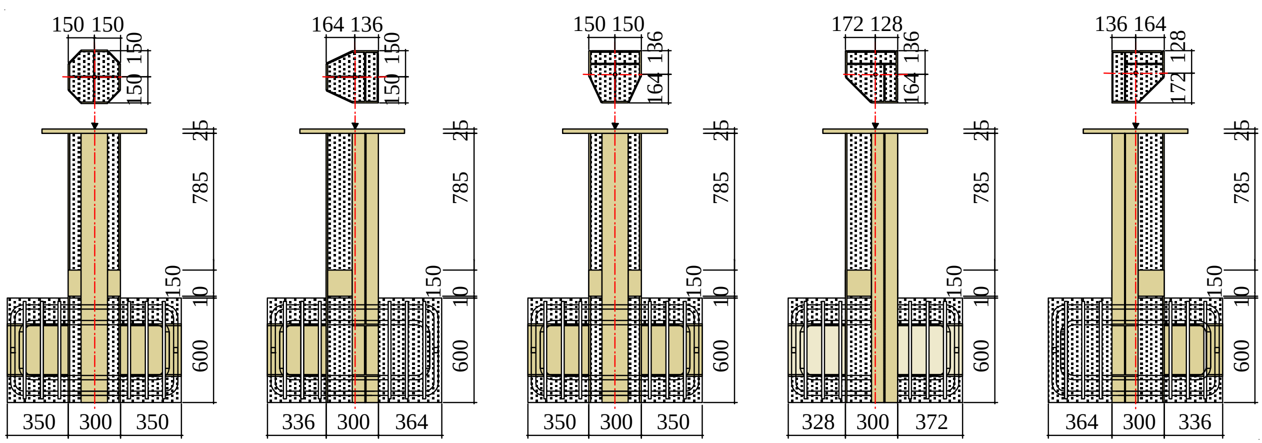


C01, C05 TX01, TX05 TY01, TY05 LX01, LX05 LY01, LY05

Fig. 2 – Test specimens (unit: mm)

Table 2 – Mechanical properties of steel and concrete

| Test series | | I | II | III |
|---|---|---|---|---|
| PL-9(SN400B, SS400) Steel flange | Yield stress (N/mm$^2$) | 292 | 308 | 326 |
| | Tensile stress (N/mm$^2$) | 426 | 433 | 453 |
| | Elongation (%) | 26.9 | 22 | 25.9 |
| PL-6.5(SN400B, SS400) Steel web | Yield stress (N/mm$^2$) | 315 | 343 | 347 |
| | Tensile stress (N/mm$^2$) | 426 | 450 | 462 |
| | Elongation (%) | 26.9 | 17.2 | 26.1 |
| PL-6(SS400) Reinforcing plate of column base | Yield stress (N/mm$^2$) | 334 | 320 | 334 |
| | Tensile stress (N/mm$^2$) | 455 | 458 | 455 |
| | Elongation (%) | 29.0 | 29.0 | 29.0 |
| Concrete | Compressive strength(N/mm$^2$) | 42.6 | 39.8 | 32.8 |
| | Cleavage strength(N/mm$^2$) | 3.02 | 2.92 | 3.38 |
| | Young's modulus (N/mm$^2$) | 30612 | 32862 | 32257 |

(i) Axial force ratio: $n=N/N_{cu}$=0.12, 0.50
(ii) Shape of the steel: cross shape, T shape, and L shape

In the nomenclature for identifying specimen types, the first character (C, T, and L) represents the shape of the column steel, the second character (X, Y) represents the load direction of the lateral force for the column section, and the number (01, 05) denotes the axial force ratio.

Both the axial force and the lateral force were added to the centroid of the column section. The mechanical properties of the steel and concrete cylinder are shown in Table 2.

All of the specimens were tested using the test setup system shown in Fig 3. The stub under the column was fixed to the loading bed. Between the loading machine and the top of the specimen, there was a rotational pin to ensure the corresponding relative displacement of the top and the bottom of the column. An axial force $N$ and a lateral force $H$ were applied by an actuator connected to the loading frame at the top of the specimen. All the specimens were subjected to a cyclic lateral force and an axial compressive force. The axial compressive load level was of two stages ($n$=0.12 or 0.50). The cyclic lateral loading was applied on every chord rotation angle $R$=0.5% radians under displacement control. The chord rotation angle $R$, shear stress of column $Q$, and bending moment of column base ${}_fM$ are given by the following equations:

$$R = \frac{\delta}{h} \tag{1}$$

$$Q = H + \frac{N \cdot \delta}{h} \tag{2}$$

$${}_fM = H \cdot h + N \cdot \delta \tag{3}$$

Where $\delta$ represents the lateral displacement of the top of the column and $h$ indicates the shear span of the column.

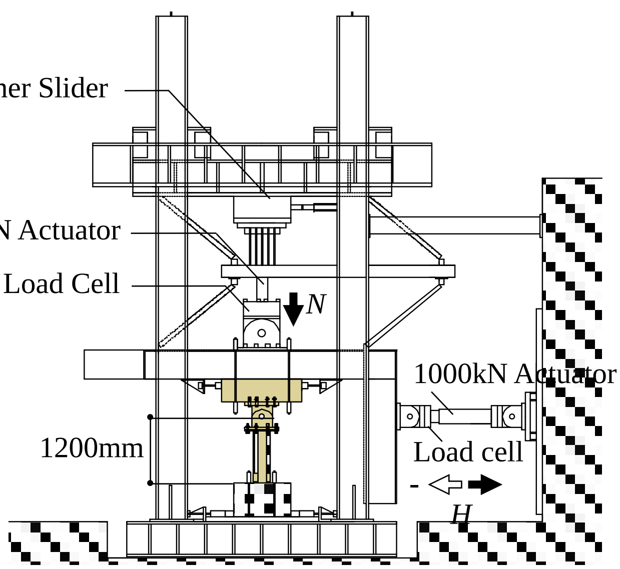

Fig. 3 – Test setup system

## 2.2 Destruction state and hysteresis characteristics

The ultimate failure states are shown in Fig. 4. The steel underwent yielding at the column base. However, a plastic zone finally developed above the reinforcing plates at the column base, and flexural failure was concentrated in this zone. Moreover, the steel flange underwent local buckling, and the concrete underwent crush. Fig. 5 shows the hysteresis curves in which the vertical axis is taken to be the lateral force *H*, and the horizontal axis is taken to be the chord rotation angle *R*. The dotted line indicates the effect of the bending moment caused by the axial force in Fig. 5. The symbol ○ represents the yielding point of steel, and the symbol △ denotes the ultimate strength of a column. Under the hysteresis characteristics of columns with a symmetrical cross section under low axial compression, it is observed that the hysteresis loop indicated a spindle-shape. Moreover, the ductility was large and the degradation of strength due to repeated loading was small. At the hysteresis characteristics of columns with an asymmetrical cross section, it is observed that the hysteresis loop indicated a spindle-shape with some pinching. However, columns under low axial compression displayed ductility. On the other hand, at the hysteresis characteristics of columns with a symmetrical cross section under a high axial compression, it is observed that the strength deterioration after the maximum carrying capacity was reached was drastic. In addition, a reduction in the deformation capacity became remarkable for columns with an asymmetrical cross section. Concrete surrounded by a steel flange could sustain a large strain due to the confining action of the flange. The area of confined concrete of the columns with an asymmetrical cross section was small compared to the columns with a symmetrical cross section. This was the why the ductility decreased after the attainment of the maximum strength.

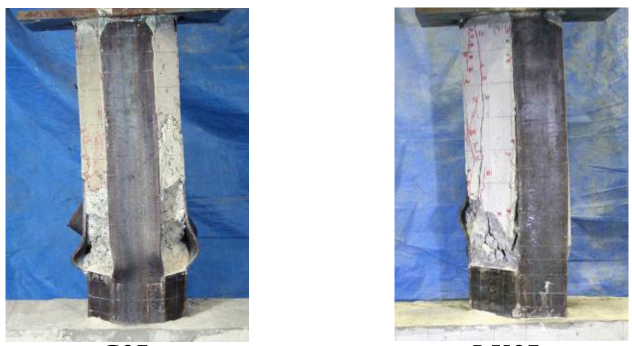

C05 LX05

Fig. 4 – Ultimate failure state

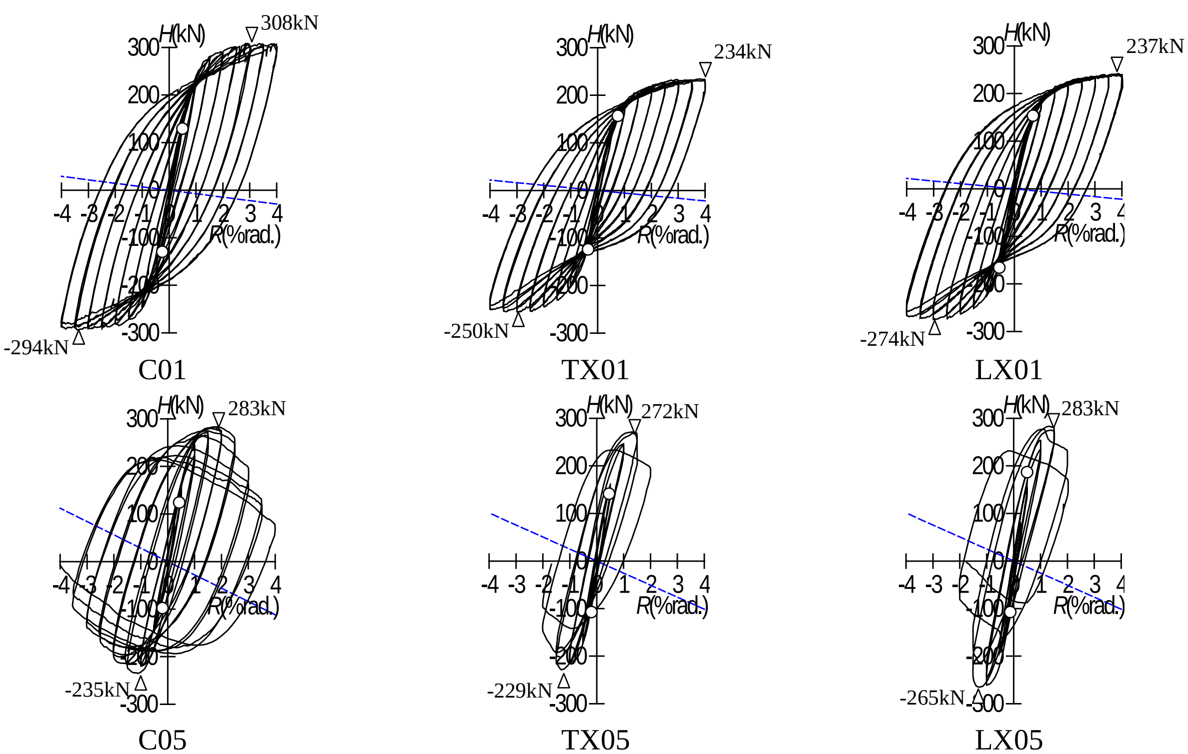

Fig. 5 – Relationships of lateral force and chord rotation angle

# 3. Ultimate flexural strength

## 3.1 The principle of superposed strength

The value of the ultimate flexural strength was calculated via the method of superposed strength as per the standard of the Architectural Institute of Japan [3], in which the ultimate strength of a section of a steel concrete composite member is taken to be the sum of the strength of a fully plastic steel section plus the ultimate strength of a concrete section. Fig. 6 shows the stress distributions of the steel under the strong-axis, the steel under weak-axis and the concrete. At the ultimate state, the following assumptions were used to generate the axial force $N$ and bending moment $M$ curve:

(i) Local buckling of the steel did not occur,
(ii) The effects of residual stresses in steel were not included, and
(iii) Tensile strength of concrete was not considered.

${}_{ss}N_u$ and ${}_{ss}M_u$: Axial force and bending moment of the steel under strong-axis
${}_{ws}N_u$ and ${}_{ws}M_u$: Axial force and bending moment of the steel under weak-axis
${}_{c}N_u$ and ${}_{c}M_u$: Axial force and bending moment of the concrete
${}_{s}\sigma_y$: Yield stress of the steel
$\sigma_c$: Compressive strength of the concrete

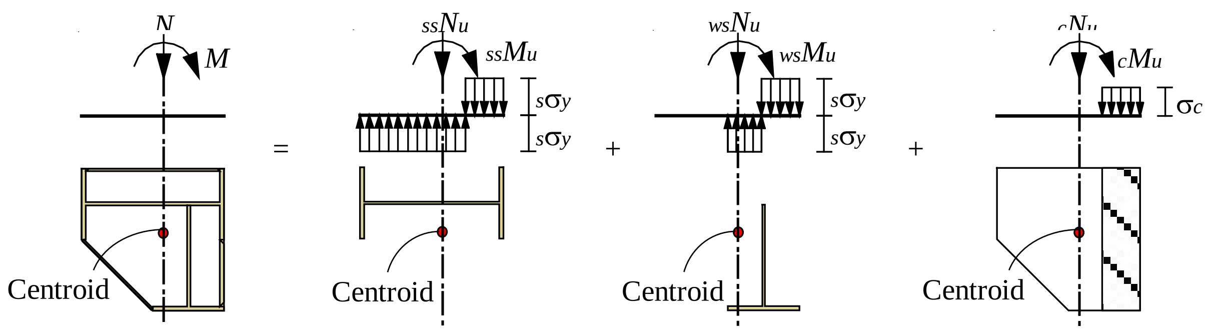


Fig. 6 – Superposed strength and stress distribution

## 3.2 Confined effect of concrete

The concrete in a steel concrete composite column was confined with steel having a cross, T, and L shape. Additionally, the concrete of the end part in the column was confined with reinforcing plates. Therefore, the compressive strength of the concrete in the steel concrete composite column increases compared with plain concrete. Equation (4) is proposed for the concrete in a concrete-filled steel tubular column of a circle section according to a recommendation by the Architectural Institute of Japan [4]:

$$\sigma_{cB} = \sigma_B + 0.78\frac{2t}{{}_{s}D - 2t}\cdot {}_{s}\sigma_y \tag{4}$$

where $\sigma_{cB}$ denotes the compressive strength of confined concrete; $\sigma_B$ represents the compressive strength of plane concrete; $t$, ${}_{s}D$ and ${}_{s}\sigma_y$ indicate the thickness, depth and yield stress of the steel tube, respectively.

## 3.3 Ultimate bending moment

Relationships of experimental values ${}_{p}M_{exp}$, ${}_{f}M_{exp}$, and the calculated values $M_u$ for all specimens are shown in Fig.7 and Fig.8. Experimental values and calculated values are shown the absolute value of the positive and negative, respectively. The relationships between axial force $N$ and ultimate bending moment $M$ for some specimens are shown in Fig.9. The compressive axial force is assumed to be positive. The solid line indicates a calculated value. The symbols denote experimental values. For the experimental values, the effect of the bending moment caused by axial force was considered. The ultimate bending moment examined the cross section at the end part in column and the upper part of reinforcing plates, respectively.

The method of the superposed strength was used for the calculations. The following assumptions were used to generate the *N*-*M* curve:

(i) Simulation I: Concrete confinement provided by steel was not considered ($\sigma_c=\sigma_B$ was assumed)

(ii) Simulation II: Concrete confinement provided by steel was considered ($\sigma_c=\sigma_{cB}$ was assumed)

In the case of Simulation I, the value in which the experimental value ${}_fM_{exp}$ was divided by the calculated value $M_u$ was 1.08～1.49 (the mean value was 1.27) for all the specimens. On the other hand, the value in which the experimental value ${}_pM_{exp}$ was divided by the calculated value $M_u$ was 0.94～1.30 (the mean value was 1.11) for all the specimens.

In the case of Simulation II, the value in which the experimental value ${}_fM_{exp}$ was divided by the calculated value $M_u$ was 0.99～1.28 (the mean value was 1.14) for all the specimens. On the other hand, the value in which the experimental value ${}_pM_{exp}$ was divided by the calculated value Mu was 0.86～1.10 (the mean value was 0.99) for all the specimens.

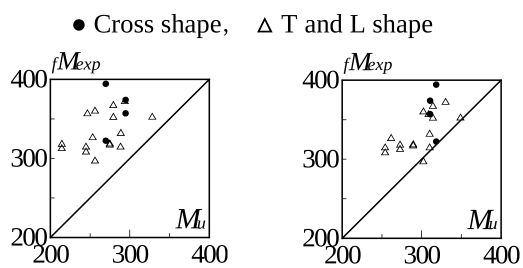


(a) Simulation I (b) Simulation II

Fig. 7 – Experimental values and calculated values (end part in column)

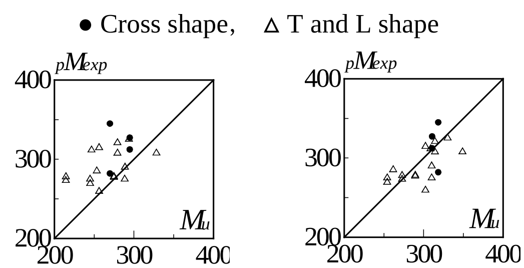


(a) Simulation I (b) Simulation II

Fig. 8 – Experimental values and calculated values (upper part of reinforcing plate)

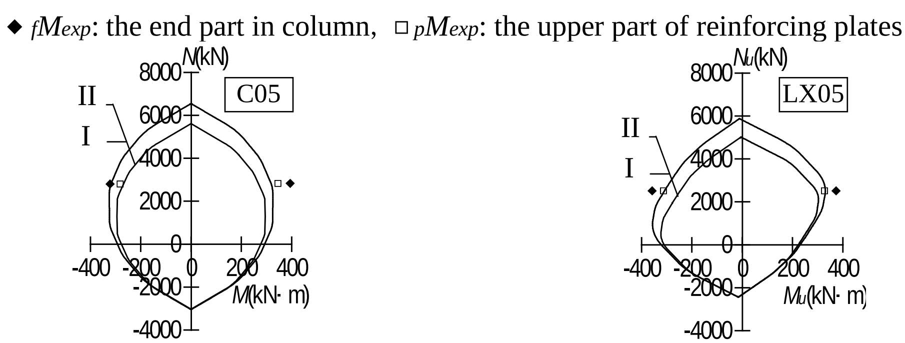


Fig. 9 – Relationships of axial force and bending moment

## 3.4 Evaluation of ultimate flexural strength

For the ultimate failure state of all the specimens in the actual experiment, a plastic zone developed above the reinforcing plates at the column base. However, the stress and strength were different at the column base section with reinforcing plates and other sections. Thus, it was necessary to examine the strength in each cross section of the column base section with reinforcing plates and other sections in the practical design. The ultimate flexural strength $Q_{mu}$ is given by the following equation:

$$Q_{mu} = \min\left(\frac{{}_fM_u}{h}, \frac{{}_pM_u}{h-l}\right) \tag{5}$$

where $l$ denotes the length of the reinforcing plates; $_fM_u$ indicates the ultimate bending moment of the end part with reinforcing plates; and $_pM_u$ represents the ultimate bending moment of the upper part of the reinforcing plates.
Table 3 lists the ultimate flexural strength. The evaluation of $_fM_u$ was calculated by using $\sigma_{cB}$. On the other hand, the evaluation of $_pM_u$ was calculated by using $\sigma_B$. It is seen from Table 3 that the experimental values $Q_{exp}$ and the calculated values $Q_{mu}$ corresponded well. The structural tests make it clear that ultimate strength can be evaluated to superposed strength method, in which the ultimate strength of the steel part and the concrete part.

Table 3 – Ultimate flexural strength

| Specimen | $_fM_{exp}$ (kN・m) | | $_pM_{exp}$ (kN・m) | | $Q_{exp}$ (kN・m) | | $_fM_u$ (kN・m) | | $_pM_u$ (kN・m) | | $_fM_u/h$ (kN・m) | | $_pM_u/(h-l)$ (kN・m) | | $Q_{exp}/Q_{mu}$ | |
|---|---|---|---|---|---|---|---|---|---|---|---|---|---|---|---|---|
| | positive | negative | positive | negative | positive | negative | positive | negative | positive | negative | positive | negative | positive | negative | positive | negative |
| C01 | 374 | -357 | 327 | -312 | 312 | -298 | 311 | -311 | 299 | -299 | 259 | -259 | 285 | -285 | 1.20 | 1.04 |
| TX01 | 316 | -333 | 276 | -291 | 263 | -277 | 254 | -310 | 248 | -296 | 212 | -258 | 236 | -282 | 1.24 | 0.98 |
| TY01 | 320 | -318 | 280 | -278 | 266 | -265 | 289 | -289 | 279 | -279 | 241 | -241 | 266 | -266 | 1.10 | 1.00 |
| LX01 | 328 | -353 | 287 | -309 | 273 | -294 | 262 | -349 | 256 | -335 | 218 | -291 | 244 | -319 | 1.25 | 0.92 |
| LY01 | 316 | -309 | 276 | -271 | 263 | -258 | 310 | -254 | 296 | -248 | 258 | -212 | 282 | -236 | 1.02 | 1.09 |
| C05 | 394 | -322 | 345 | -282 | 329 | -269 | 318 | -318 | 285 | -285 | 265 | -265 | 271 | -271 | 1.24 | 0.99 |
| TX05 | 368 | -314 | 322 | -275 | 307 | -261 | 314 | -273 | 292 | -232 | 262 | -227 | 278 | -221 | 1.17 | 1.15 |
| TY05 | 361 | -298 | 316 | -261 | 301 | -248 | 302 | -302 | 270 | -270 | 252 | -252 | 257 | -257 | 1.20 | 0.97 |
| LX05 | 373 | -358 | 327 | -313 | 311 | -298 | 330 | -309 | 307 | -265 | 275 | -257 | 292 | -252 | 1.13 | 1.16 |
| LY05 | 319 | -353 | 279 | -309 | 266 | -294 | 273 | -314 | 232 | -292 | 227 | -262 | 221 | -278 | 1.20 | 1.06 |

# 4. Evaluation of restoring force characteristics

## 4.1 Analytical model

(1) Skelton Curve

A skelton curve of restoring force characteristics for the proposed steel concrete composite columns under flexural failure is shown in Fig. 10. This model is composed of three characteristic points, namely the bending crack initiation point ($R_c$, $Q_c$), the flexural yield point ($R_y$, $Q_y$), and the maximum bending moment point ($R_u$, $Q_u$). For the ease of calculation, the concrete part for a polygonal-section was replaced with a rectangular-section to which values of cross section and section modulus were equal.
Meanwhile, $Q_c$ (=$Q_{mc}$) is given by following equation:

$$Q_c = \frac{M_c}{h} \tag{6}$$

$$M_c = \left(\sigma_t + \frac{N}{A_e}\right) \cdot Z_e \tag{7}$$

where $\sigma_t$ represents the tensile strength of concrete; and $A_e$ and $Z_e$ denote the equivalent cross-sectional area and equivalent section modulus which considers steel part, respectively.
Meanwhile, $R_c$ is given by equation (8). Evaluation of the initial stiffness $K$ is done using the elastic bending

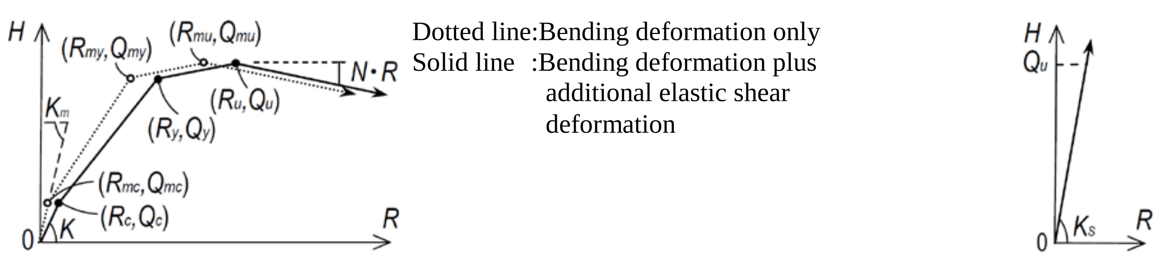

（a）Flexural and shear deformation （b）Additional elastic shear deformation

Fig. 10 – Skelton Curve

stiffness $K_m$ and the elastic shear stiffness $K_s$.

$$R_c = \frac{Q_c}{K \cdot h} \tag{8}$$

$$K = \frac{K_m \cdot K_s}{K_m + K_s} \tag{9}$$

$$K_m = \frac{3 {}_cE^{*} \cdot I_e}{h^3} \tag{10}$$

$$K_s = \frac{{}_cG \cdot {}_cA + {}_sG \cdot {}_sA_s}{\kappa \cdot h} \tag{11}$$

where ${}_cE^*$, ${}_cG$, and ${}_cA$ represent the tangent modulus, elastic shear modulus, and cross-sectional area of concrete, respectively; $I_e$ denotes the equivalent geometrical moment of inertia which considers the steel section; and ${}_sG$ and ${}_sA_s$ indicate the elastic shear modulus and cross-sectional area of steel, respectively. Note that ${}_sA_s$ is a cross-sectional area that only considers the shear resistance element. Finally, $\kappa$ denotes a coefficient which is related to shear deformation ($\kappa$=1.2) and ${}_cE^*$ is given by the following equation [5]:

$$ {}_cE^* = \left. \frac{d{}_c\sigma({}_c\varepsilon)}{d{}_c\varepsilon} \right|_{{}_c\varepsilon = \varepsilon_N} \tag{12}$$

$$N = {}_sA \cdot {}_sE \cdot \varepsilon_N + {}_cA \cdot {}_c\sigma(\varepsilon_N) \tag{13}$$

where ${}_c\sigma$ and ${}_c\varepsilon$ denote the stress and strain of concrete; $\varepsilon_N$ represents the strain by the action of the axial force only; and ${}_sA$ and ${}_sE$ indicate the cross-sectional area and Young's modulus of steel, respectively.

$Q_y$ (=$Q_{my}$) is given according to a standard of the Architectural Institute of Japan [3].

Meanwhile, $R_y$ is calculated by adding the elastic shear deformation $R_{sy}$ (=$Q_y/K_s$) to $R_{my}$, where $R_{my}$ is given by a standard of the Architectural Institute of Japan [3].

$Q_u$ (=$Q_{mu}$) is given by equation (5). The restoring force after the attainment of the maximum strength decreases due to the effect of overturning moment by the axial force.

$R_u$ is calculated by adding elastic shear deformation $R_{su}$ (=$Q_u/K_s$) to $R_{mu}$, where $R_{mu}$ is given by a standard of the Architectural institute of Japan [3].

(2) Unloading and reloading

Unloading and reloading before a bending crack occurs is calculated using Equations (8)-(11). Meanwhile, unloading and reloading after a bending crack occurs is calculated by Fujimoto's model [6]. This model was proposed for steel concrete composite columns where fiber-reinforced concrete is used. The unloading-stiffness $K_r$ shown in Fig. 11 is given by following equation:

$$K_r = K \cdot \left| \frac{R_m}{R_c} \right|^{-\alpha} \tag{14}$$

$$\alpha = -2 \frac{{}_sA}{bD} + 0.58 \tag{15}$$

Where $R_m$ denotes the maximum chord rotation angle; $\alpha$ represents the unload-stiffness coefficient; and $b$ and $D$ denote the width and depth of the column.

Fig. 12 shows the relationships between $R_m$ and $\alpha$. The symbols are determined experimentally. The dotted and solid lines are given by Equation (15). It is clear that the identified and calculated values are almost equal.
Fig. 13 shows the model of reloading after unloading. $R_m$ and $H_m$ denote the maximum chord rotation angle point. Meanwhile, $\beta$ indicates the strength ratio of the point at which the stiffness changes and is determined experimentally as shown in Fig. 14. Fig. 15 shows the relationship between $R$ and $\beta$. The symbols are determined experimentally.

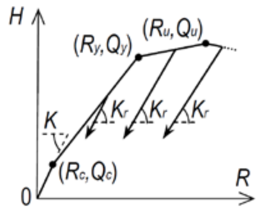


Fig. 11 – Unload-stiffness

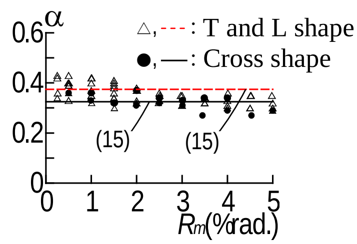


Fig. 12 – Unload-stiffness coefficient

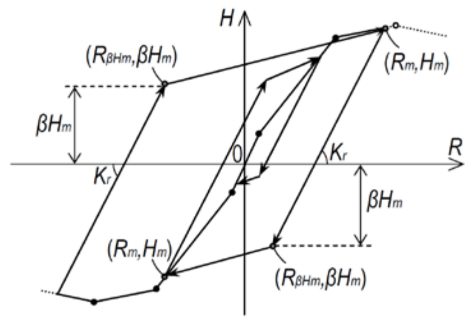


Fig. 13 – Reload after unload

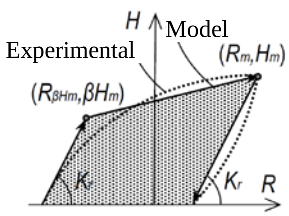


Fig. 14 – Equivalent area

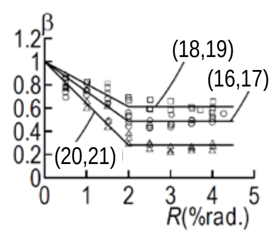


Fig. 15 – Strength ratio of stiffness changes point ($n$=0.1)

The approximation of the identified values is given by following equation:

(i) Shape of the column: symmetrical cross section

$$R \leq 0.02\text{rad.} \qquad \beta = -25.7R_m+1.00 \tag{16}$$

$$R > 0.02\text{rad.} \qquad \beta = 0.486 \tag{17}$$

(ii) Shape of the column: asymmetrical cross section (lateral load: direction of low strength from high strength)

$$R \leq 0.02\text{rad.} \qquad \beta = -19.4R_m+1.00 \tag{18}$$

$$R > 0.02\text{rad.} \qquad \beta = 0.612 \tag{19}$$

(iii) Shape of the column: asymmetrical cross section (lateral load: direction of high strength from low strength)

$$R \leq 0.02\text{rad.} \qquad \beta = -36.0R_m+1.00 \tag{20}$$

$$R > 0.02\text{rad.} \qquad \beta = 0.280 \tag{21}$$

## 4.2 Discussion on the analytical results

Fig. 16 shows the relationship between $H$ and $R$ (Simulation I). In these figures, the solid lines indicate the analytical value and the dotted lines represent the experimental value. The analytical values predict the experimental results before local buckling of the steel flange and crush of compression concrete occur. However, when the experimental results of ultimate strength do not correspond to the calculated values, there is a difference in the restoring force property of the experimental results and analytical values. Therefore, the restoring force which used the experimental value of ultimate strength instead of the analytical value of the ultimate strength (Simulation II) was calculated. In this simulation (refer to Fig. 17), the proposed analytical model of the restoring force property was in accordance with the test results.

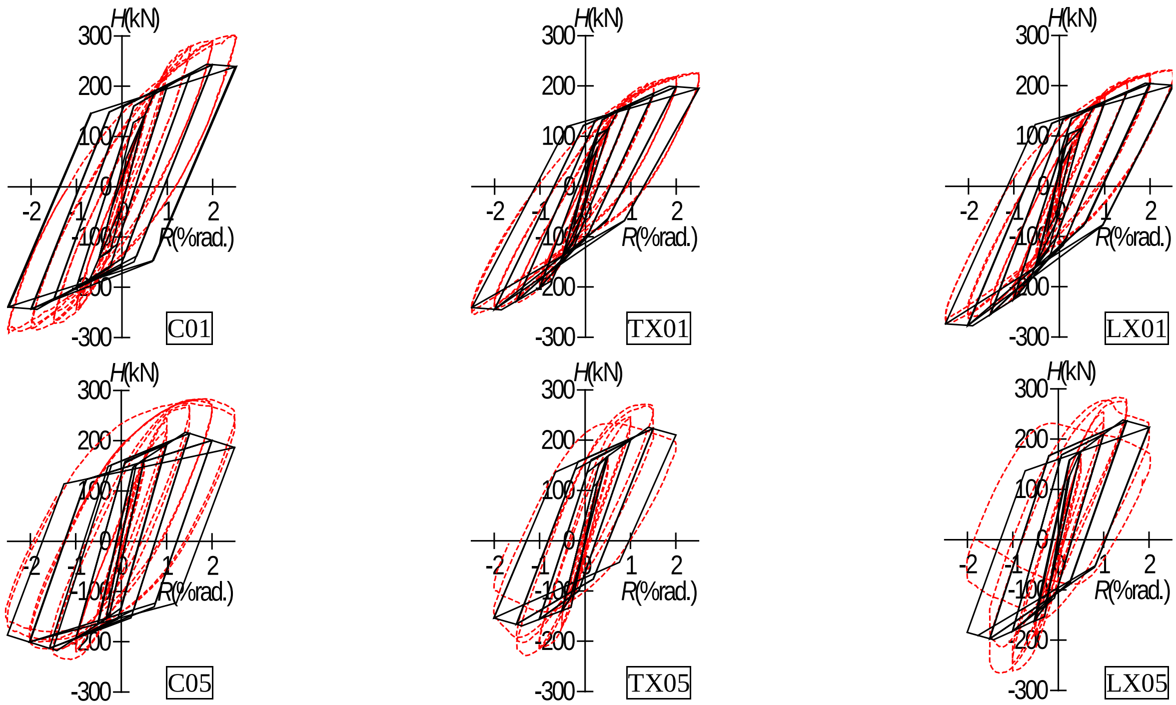


Fig. 16 – Analytical results (Simulation I)

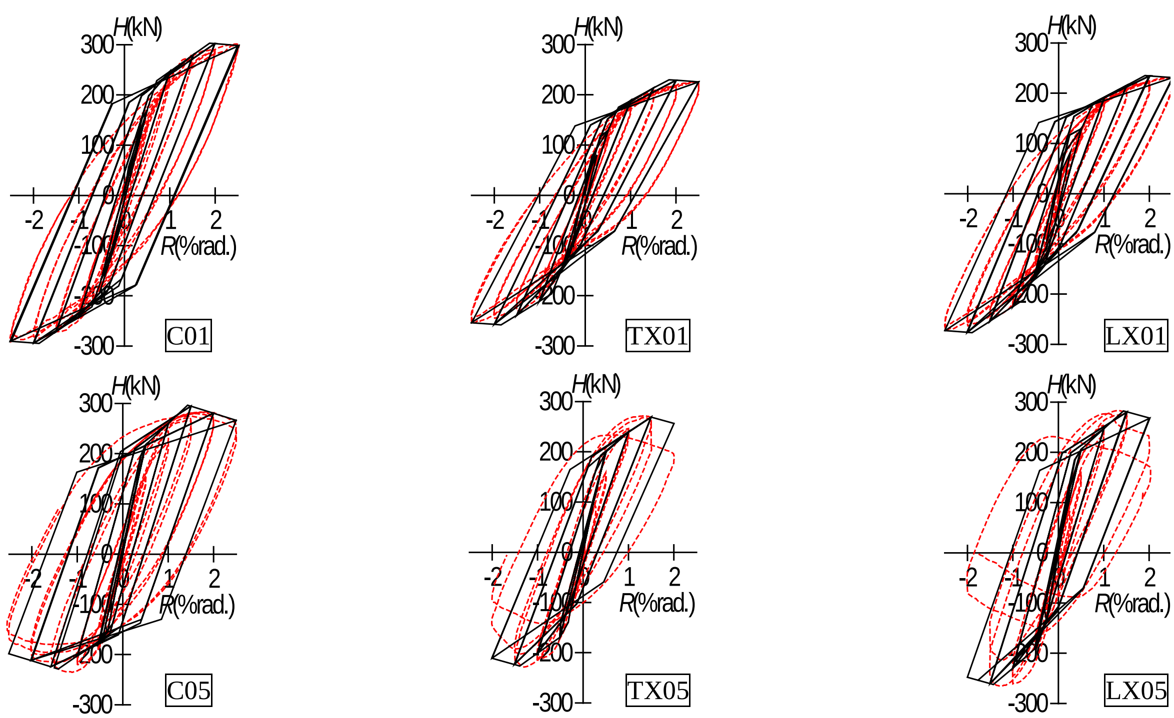

Fig. 17 – Analytical results (Simulation II)

## 5. Conclusions

Structural tests were carried out to study the mechanical properties of columns in steel concrete composite structures subjected to a repeated bending moment under an axial compressive force. The following was observed from the test results:

1). For the ultimate failure state, a plastic zone developed above the reinforcing plates and flexural failure was concentrated in this zone.

2). Compared to the columns with a symmetrical cross section, a reduction in the deformation capacity became remarkable for the columns with an asymmetrical cross section under a high axial force.

3). The ultimate strength can be evaluated by the superposed strength method, in which the ultimate strength of the steel part and the concrete part respectively.

4). The proposed analytical model of the restoring force property is in good accordance with the test results.

## 6. References

[1] MINAE F. and Koichi M. (2008): Seismic Performance of New Type Steel-Concrete Composite Structures Considering Characteristic both SRC and CFT Structures, *14th World Conference on Earthquake Engineering*, Paper ID 12-01-0017, Beijing, China.

[2] Kazushi S., Katsuya A. and Koichi M. (2012): Ultimate Strength and Restoring Force Characteristics of Unembedded Type Column Bases in Steel-Concrete Composite Structures, *15th World Conference on Earthquake Engineering*, Paper’s Number:0185, Lisbon, Portugal.

[3] Architectural Institute of Japan (2014): AIJ Standard for Structural Calculation of Steel Reinforced Concrete Structures.

[4] Architectural Institute of Japan (2008): Recommendations for Design and Construction of Concrete Filled Steel Tubular Structures.

[5] Go N., Takashi F., Isao M. and Yasuhiro O. (2003): Model for the Skeleton Curve of Square CFT Beam-Columns, *Concrete Research and Technology, Vol. 14, No. 2*, pp.31-41.

[6] Toshiaki F., Hiroshi K. and Tomoya M. (2009): Structural Performance Evaluation for CES Columns with Cross-H-Shaped Steel, *11th Symposium Research and Application of Hybrid and Composite structures*, pp.4-1-4-8.